Factors controlling inter-catchment variation of mean transit time with consideration of temporal variability

Wenchao Ma and Tsutomu Yamanaka, Center for Research in Isotopes and Environmental Dynamics, University of Tsukuba, Japan; Faculty of Life and Environmental Sciences, University of Tsukuba, Japan

Corresponding author:

Wenchao Ma E-mail: wma@ied.tsukuba.ac.jp

Phone: +81-29-852-2533

Address: 1-1-1 Tennoudai, Tsukuba, Japan

TsutomuYamanaka E-mail: tyam@geoenv.tsukuba.ac.jp

Phone: +81-29-853-2538

Address: 1-1-1 Tennoudai, Tsukuba, Japan

Abstract:

The catchment transit time, a lumped descriptor reflecting both time scale and spatial structure of catchment hydrology can provide useful insights into chemical/nuclear pollution risks within a catchment. Despite its importance, factors controlling spatial variation of mean transit time (MTT) are not yet well understood. In this study, we estimated time-variant MTTs for about ten years (2003–2012) in five

mesoscale sub-catchments of the Fuji River catchment, central Japan, to establish the factors controlling their inter-catchment variation with consideration of temporal variability. For this purpose, we employed a lumped hydrological model that was calibrated and validated by hydrometric and isotopic tracer observations. Temporal variation patterns of estimated MTT were similar in all sub-catchments, but with differing amplitudes. Inter-catchment variation of MTT was greater in dry periods than wet periods, suggesting spatial variation of MTT is controlled by water 'stock' rather than by 'flow'. Although the long-term average MTT (LAMTT) in each catchment was correlated with mean slope, coverage of forest (or conversely, other land use types), coverage of sand–shale conglomerate, and groundwater storage, the multiple linear regression revealed that inter-catchment variation of LAMTT is principally controlled by the amount of groundwater storage. This is smaller in mountainous areas covered mostly by forests and greater in plain areas with less forest coverage and smaller slope. This study highlights the topographic control of MTT via groundwater storage, which might be a more important factor in mesoscale catchments, including both mountains and plains, rather than in smaller catchments dominated by mountainous topography.

Keywords: transit time; catchment hydrology; tank model; isotope tracer; Fuji River

1. Introduction

Given a scenario of a water pollution accident, such as that following a nuclear bomb, it is imperative to know how long it would take the polluted water to reach any specific location, especially sources of domestic water supply systems. The catchment transit time, which is defined as the elapsed time from when a water molecule enters a catchment across the land surface until it exits at the catchment outlet through the

stream network (Bolin and Rodhe, 1973; McDonnell et al., 2010), has been one of the major research topics in the field of catchment hydrology. It reflects the storage, flow pathway, and sources of water within the catchment, in addition to how the catchment retains and releases water (McGuire and McDonnell, 2006). Therefore, knowledge of the catchment transit time can provide useful insights with regard to taking prompt appropriate measures against chemical/nuclear pollution events.

As the transit time differs for each individual water molecule, we have to consider the mean transit time (MTT) and transit time distribution (TTD) for a mass of water molecules. In earlier works (Maloszewski and Zuber, 1982; Maloszewski et al., 1983; DeWalle et al., 1997; Ozyurt and Bayari, 2003), MTT has usually been estimated by modeling input–output relationships of conservative tracers such as stable isotopes or chloride under the assumption of steady-state and using hypothetical TTD functions. These simple treatments for estimating MTT have become controversial and new methods based on time-variant TTDs or without an explicit form of TTD have been developed to estimate MTT (McGuire et al., 2002; Sayama and McDonnell, 2009; Duffy, 2010; Ma and Yamanaka, 2013). These studies demonstrated that TTDs can change rapidly over time and through responding to rainfall and drought events, they are highly irregular in shape, which introduces considerable temporal variability to the MTT. Recently, other tracers were newly applied to relative research destinations. Such as, nutrient was testified identifiable during hydrological and biogeochemical responses (Hrachowitz et al., 2015), as well as Fovet et al., (2014) estimated the nitrogen transit time in headwater catchment; Peters et al., (2014) combine used groundwater $^{3}H/^{3}He$ ages and dissolved silica (Si) concentrations for investigating mean streamwater transit time; hexavalent chromium (Cr(VI)) and chromium hydroxide (Cr(OH)3(s)) were used by Druhan and Maher (2014) in structurally correlated subsurface heterogeneous porous media.

Hydrological variations are generally introduced by many factors such as climate, soil and soil water transit time were carried out by Tetzlaff et al. (2014), Kim and Jung (2014), Stockinger et al., (2014), Timber et al., (2015), vegetation, topography, geology, snow (Seeger and Weiler, 2014), and anthropogenic activities (Blöschl, 2005). Therefore, catchment transit time is variable in space. Previous studies reported that MTT depends upon topography (McGuire et al., 2005), soil (Soulsby et al., 2006a), or both (Soulsby et al., 2006b; Tetzlaff et al., 2009; Hrachowitz et al., 2010). However, the correlation between MTT and catchment size was not obvious, while inter-catchment variance of MTT decreased with increasing catchment size (Soulsby et al., 2006a; Hrachowitz et al., 2010). Although these studies clarified the factors controlling transit time, the temporal variabilities of MTT and TTD were not considered in their analyses and thus, the understanding of the inter-catchment variation of time-variant MTT and its controlling factor(s) is incomplete. McDonnell et al. (2010) stated as one of four research needs: "We need more work that relates transit times to geographic, geomorphic, geologic, and biogeochemical characteristics of catchments." Stream MTTs in tropical montane regions (Muñoz-Villers et al., 2015), and temporal dynamics of catchment transit times (Klaus et al., 2014) related to catchment characteristics were discussed, and both of these researches were carried out in small catchment.

The objectives of the present study are to compare MTTs among catchments with consideration of their temporal variability and to establish the factors controlling inter-catchment variation. A lumped hydrologic model, which was calibrated/validated with hydrometric and isotopic measurements (Ma and Yamanaka, 2013) was employed for this purpose. Here, we focus on mesoscale catchments. Mesoscale catchments are commonly associated with anthropogenic activities and thus, they are often of great interest regarding the development of water resources and interventions intended to enhance rural livelihoods (Love et al., 2011). Nevertheless, in mesoscale catchments, hydrological processes occurring on smaller scales develop in

complex ways to produce an integrated response (Scherrer and Naef, 2003; Uhlenbrook et al., 2004), such that storm–runoff generation on the mesoscale has not yet been clarified. Therefore, studies on mesoscale catchments are both significant and imperative.

2. Material and methods

2.1 Site description

The catchments investigated in this study are five sub-catchments (SCs) comprising the Fuji River catchment (35.5–36.0°N, 138.2–138.9°E), central Japan (Fig. 1). The area of the total (i.e., Fuji River) catchment is 2172.7 km^2 and its elevation ranges from approximately 234.7 to 2962.8 m. Annual precipitation is about 1135.2 mm, mean relative humidity is 65%, mean temperature is 14.7 °C, and the mean wind speed is 2.2 ms^{-1} (based on records of meteorological observations between 1981 and 2010 at Kofu station, operated by the Japan Meteorological Agency (JMA)). Northern, eastern, and western parts of the catchment are characterized by mountainous topography, whereas the central and southern areas are alluvial fans and lowlands. The mountains are formed mostly by granite and partly by andesitic/basaltic rocks. The following geological compositions were found within the study area and taken into consideration: basalt of undefined geological time (Ba), welded tuff of Quaternary age (Wt), sand–shale conglomerate of Mesozoic age (Ss), and granite of undefined geological time (Gr). Forest is the dominant land-use type over the entire study area with its percentage coverage ranging from 67% to 94%. The residual percentages are mainly given over to agricultural land and range grassland. The land use/land cover is mainly formed by forests in the mountainous areas, orchards and vegetable fields in the alluvial fans, and residential areas and paddy fields in the alluvial lowlands. The five SCs were defined with consideration of the location of

gauging stations maintained by the Ministry of Land, Infrastructure, Transport, and Tourism.

2.2. Data

For the period from January 1, 2006 to September 30, 2012, AMeDAS (Automatic Meteorological Data Acquisition System) radar precipitation data produced by the JMA were used to consider the spatial variability of precipitation. These data provide maps of hourly accumulations of precipitation estimated from combined observations from radars and rain gauges (e.g., see Makihara, 1996). The spatial resolution is approximately 1 × 1 km. Before this period (i.e., 2003–2005), point precipitation data from hydro-meteorological stations were used and the Thiessen polygon method applied to obtain areal mean precipitation in each SC. The locations of the hydro-meteorological stations are shown in Fig. 1.

Data of observed daily river discharge produced by the Ministry of Land, Infrastructure, Transport, and Tourism (MLIT) were used for each SC. For calculating the evapotranspiration, we applied the FAO Penman–Monteith method (Allen et al., 1998). Meteorological data (solar radiation, air temperature, relative humidity, and wind speed) observed by the JMA at three weather stations (Fig. 1) were used. Based on the relationships between the elevation of the stations and the meteorological variables, representative values were estimated considering the mean elevation of each SC, which were then used for the evapotranspiration computation. Here, temperature was regressed considering elevation affect, around -0.57 °C difference of 100 meter elevation increased for the local catchment. For other meteorological parameters, we applied values at a nearest station for the whole catchment. (Figure 1.)

In addition to the existing data set, we performed monthly isotopic monitoring of river water at the Ministry of Land, Infrastructure, Transport, and Tourism gauging stations from April 2010 (or April 2011) to

March 2012. Monthly monitoring of the precipitation isotope was also performed at Kofu (Fig. 1). A precipitation collector (Shimada et al., 1992, Yamanaka et al., 2004) that can prevent the evaporation of stored precipitation was used for collecting monthly precipitation, and the mixed value representing average of precipitation isotope composition for the relative month (Ma and Yamanaka, 2013). Hydrogen and oxygen stable isotope ratios ($^{2}H/^{1}H$ and $^{18}O/^{16}O$) of the collected water samples were measured using a tunable diode laser isotope analyzer (L11020-I, Picarro, CA, USA). The measurement errors for this analyzer were 0.1‰ for $\delta^{18}O$ and 1‰ for δD (Yamanaka and Onda, 2011). For each SC, the mean values of $\delta^{18}O$ and δD of precipitation were estimated considering regional altitudinal effects (1.6‰/100 m for $\delta^{18}O$ and 6.4‰/100 m for δD), which were determined from the data set of Makino (2013).

3. Theory

The lumped hydrologic model for estimating time-variant MTT (and TTD) has been successfully applied in the Fuefuki River catchment (Ma and Yamanaka, 2013). However, the applicability of this model to other catchments is still unknown; therefore, in this study, we applied it to the five SCs of the Fuji River catchment, which includes the Fuefuki River catchment (SC3). The detailed equations of this tracer-aided tank model were not provided in the main text of Ma and Yamanaka (2013); therefore, we outline the principal specific steps here.

3.1 Water balance

The model is composed of five tanks in series vertically, where the water flow within each conceptually represents the overland flow, rapid throughflow, delayed throughflow, groundwater flow, and in-bedrock flow, respectively (Fig. 2). The model was initialized by spin-up with the initial two years data. Total runoff

Q, horizontal water flux (strictly, towards a stream network) [$q_H(i)$), and vertical water flux [$q_V(i)$] for the i-th tank can be computed by the following equations in daily steps, respectively:

$$Q = \sum_{i=1}^{5} q_H(i) \tag{1}$$

$$q_H(i) = \max\left[k_H(i)\left(h(i) - h_H(i)\right), 0\right], \tag{2}$$

$$q_V(i) = \max\left[k_V(i)\left(h(i) - h_V(i)\right), 0\right], \tag{3}$$

where $h(i)$ is the water level in the i-th tank, $h_V(i)$ is the level of the top of the vertical pipes connecting the bottom outlets, $h_H(i)$ is the level of the lateral outlets, and $k_V(i)$ and $k_H(i)$ are the conductance parameters analogous to the hydraulic coefficients of Darcy's law, which regulate $q_V(i)$ and $q_H(i)$, respectively. Furthermore, the differences between $h(i)$ and $h_V(i)$ or $h_H(i)$ correspond to the hydraulic gradient. The magnitude of $\Delta h_{H\text{-}V}$ [$\equiv h_H(i) - h_V(i)$; > 0, in normal cases] controls the relative importance of the horizontal and vertical flows within each layer, such that the values of $k_V(i)$, $k_H(i)$, and $\Delta h_{\text{H-V}}$ are determined through calibration based on the comparison of the observed and predicted hydrographs.

One of the simplifications in this method is that water level (i.e., analogous to potential) in a lower tank does not affect flow from an upper tank and that the flow direction is always downward. This permits the avoidance of an iteration procedure in computing fluxes and potentials and thus, the computation time can be reduced markedly. Similarly, for the horizontal fluxes (or runoff components), water level in a stream channel is not considered, and the scale of the distance between the stream channel and a point at which the hydraulic status is represented by the water level in the tank is unknown. This vague expression does introduce uncertainties, mainly in the determination of conductance parameters $k_H(i)$, but it might implicitly represent the variable source area concept.

Water budget equations for the 1st and the other four tanks are given as follows, respectively:

$$\frac{dh(i)}{dt} = P - I - f_T(i)T_r - f_E(i)E_S - q_V(i) - q_H(i) \qquad \text{for } i=1, \tag{4}$$

$$\frac{dh(i)}{dt} = q_V(i-1) - f_T(i)T_r - f_E(i)E_S - q_V(i) - q_H(i) \qquad \text{for } i=2\text{-}5, \tag{5}$$

where t is time, P is precipitation, I is interception loss, T_r is transpiration, E_s is soil evaporation, and $f_T(i)$ and $f_E(i)$ are weighting factors at the i-th tank for root water uptake and soil evaporation, respectively. We assume $I = f_I P$, and the f_I value were set as 0.164, 0.133, 0.118, 0.117 and 0.151 for each catchment considering the percentage of land use and vegetation, and the ratios following previous work on humid temperate forests (Sugita and Tanaka, 2009). Evapotranspiration, ET (= $T_r + E_s + I$), is estimated as

$$ET = K_c ET_0, \tag{6}$$

where K_c is the single-crop coefficient and ET_o is the reference evapotranspiration obtained from the FAO Penman–Monteith equation (Allen et al., 1998). We applied the value of K_c (= 1) for conifer trees. According to Kubota and Tsuboyama (2004), the proportion of soil evaporation to total evapotranspiration in forests generally ranges from 3% to 20% with an average of 10%. Thus, we assign E_s and T_r as follows:

$$E_S = \max\left[F_E ET,\ 0\right], \tag{7}$$

$$T_r = \max\left[ET - I - E_S,\ 0\right], \tag{8}$$

where F_E (=0.1 in the present study) is E_S/ET. In forests in central Japan, the zone of root water uptake is usually <50 cm beneath the ground surface, although some species do take up water from soil at depths >1 m (Yamanaka et al., 2009). Therefore, we assumed $f_T(1, 2, 3, 4, 5) = (0, 0.7, 0.3, 0, 0)$. In addition, we assumed that soil evaporation does not occur in the deeper tanks, i.e., $f_E(3, 4, 5) = (0, 0, 0)$. The values for $f_E(i)$ in the shallower tanks depend on the amount of water in the tank, as follows:

$$f_E(1) = \begin{cases} 1 & \text{for} \quad h(1)^t > 0 \\ 0 & \text{for} \quad h(1)^t \le 0 \end{cases}, \tag{9}$$

$$f_E(2) = \begin{cases} 1 & \text{for} \quad h(2)^t > 0 \\ 0 & \text{for} \quad h(2)^t \le 0 \end{cases}, \tag{10}$$

where superscript "*t*" means the value for the subsequent time step.

Although $f_T(i)$, $f_E(i)$, $f_I(i)$, $K_c(i)$, and $F_E(i)$ should depend on land use type and/or vegetation condition, we set the values for typical forests within the study area because forest is the most dominant land cover within most of the studied catchments.

3.2 Isotope balance

For the water balance calculation, water fluxes are decided by $h(i) - h_H(i)$ and $h(i) - h_V(i)$, as shown by equations (2) and (3). This means that only the value $h_H(i) - h_V(i)$ can be calibrated by hydrographs, and the absolute values of $h_H(i)$ and $h_V(i)$ cannot been fixed. However, isotope data allows for calibrating them, because concentration of tracers depends on absolute volume of water reservoir rather than on hydraulic gradient. In other words, use of hydrograph alone (without isotopes) cannot constrain tank parameters, providing worse estimates of MTT. The values of $h_V(i)$ or $h_H(i)$ also regulate isotope mixing within each tank, as described below. This is the reason why we modeled not only water balance, but also isotope balance. The isotopic composition is assumed to well mixed instantaneously within each tank.

Referring to the relevant water balance component, the isotopic composition of total runoff δ_Q can be obtained as:

$$\delta_Q = \frac{\sum_{i=1}^{5} q_H(i)\delta_w(i)}{Q}, \tag{11}$$

where δ is the isotopic composition (i.e., $\delta^{18}O$ or δD) and values of $h_V(i)$ are determined by comparing the

predicted and observed δ_Q. In the type of tank model commonly used for predicting only runoff, $h_V(i) = 0$ is assumed. Determination $h_V(i)$ is less sensitive to hydrograph, but more sensitive to isotopic tracers.

The isotope budget equation in each tank is expressed as follows:

$$\frac{dh(i)\delta_w(i)}{dt} = (P-I)\delta_P - \left[f_T(i)T_r + q_V(i) + q_H(i)\right]\delta_w(i) - f_E(i)E_S\delta_E \qquad \text{for } i=1, \tag{12}$$

$$\frac{dh(i)\delta_w(i)}{dt} = q_V(i-1)\delta_P - \left[f_T(i)T_r + q_V(i) + q_H(i)\right]\delta_w(i) - f_E(i)E_S\delta_E \qquad \text{for } i=2\text{-}5, \tag{13}$$

where subscripts P, E, and w denote precipitation, soil evaporation, and water, respectively, in each tank. Instantaneous and complete mixing within each tank is assumed in this model. The value of δ_E can be obtained by the following Craig–Gordon model (Craig and Gordon, 1965; Gat et al., 1996), and the kinetic fractionation $\Delta\varepsilon$ is defined as:

$$\delta_E = \frac{\delta_w(i)/\alpha - h_a\delta_a - (1-1/\alpha)\times 10^3 - \Delta\varepsilon}{1 - h_a + \Delta\varepsilon/10^3} \qquad \text{for } i=1 \text{ or } 2, \tag{14}$$

$$\Delta\varepsilon = (1-h_a)\frac{\rho_M}{\rho}\left[(D/D_i)^n - 1\right]\times 10^3, \tag{15}$$

where α is the equilibrium isotopic fractionation factor as a function of temperature (for experimental functions, see Majoube (1971)), h_a is the relative humidity of air, and δ_a is the isotopic composition of atmospheric water vapor. The parameter $\rho_{M,}$ is the resistance to molecular diffusion of water vapor, ρ is the total resistance to water vapor transfer from the evaporating surface to the air, D is the water vapor diffusivity in the air, D_i is the water vapor diffusivity for heavy isotopes, and n is a semi-empirical parameter (=1/2 for fully turbulent conditions). According to the experimental results of Cappa et al. (2003), D/D_i is equal to 1.0319 for oxygen and 1.0164 for hydrogen. A representative value of ρ_M/ρ is 0.32 (Yamanaka, 2009). Strictly, h_a is the vapor pressure normalized by the saturation vapor pressure at the temperature of the evaporating surface rather than air temperature; however, we used relative humidity in the common sense

for convenience.

After the values of $h_V(i)$ or $h_H(i)$ were determined, the storage of each layer of each SC was calculated as the thickness of each tank; thus, total storage was considered as the sum of the storage over all the layers.

3.3 Calibration and validation

Calibrations of the model parameters were made considering the Nash–Sutcliffe Efficiency (*NSE*) for water balance. The *NSE* is a normalized statistic that determines the relative magnitude of the residual variance ("noise") compared with the measured data variance ("information") (Nash and Sutcliffe, 1970), and it is represented by the following equation:

$$NSE = 1 - \left[\sum_{i=1}^{n} \left(Y_i^{obs} - Y_i^{sim} \right)^2 / \sum_{i=1}^{n} \left(Y_i^{obs} - Y_i^{mean} \right)^2 \right], \quad (16)$$

where Y is the runoff, and super scripts *obs*, *sim*, and *mean* denote the observed, simulated, and mean values, respectively. For isotope balance, the root mean square error (*RMSE*) rather than *NSE* was used for calibration, because the measured data variance of river water isotopic composition is very small. The *NSE* was used for calibrating k_H, k_V, and $\Delta h_{H\text{-}V}$, and then the *RMSE* was used for h_H (and thus, h_V).

To obtain the optimal combination of values of the model parameters, the Monte Carlo simulation was employed. This method performs random sampling of parameter values from a possible range, followed by model evaluations using *NSE* and *RMSE* for a set of the sampled values. The possible range was set to be ±5% around the newest optimal value for each parameter in the iteration calculations. In the procedure of calibration for isotope balance, the combined-*RMSE* ($\equiv \{RMSE_{\delta D}/8 + RMSE_{\delta 18O}\}/2$) was used for selecting the best parameter set for both $\delta^{18}O$ and δD, because a set of parameters providing the best result for $\delta^{18}O$ is not always the best for δD, and vice versa. The contribution of δD was divided by 8, according to theory of GMWL, and the average value were used for representing combined use of $\delta^{18}O$ and δD. Here we used

RMSE rather than NSE as a measure of model performance, because variation range of isotopic data is relatively small and thus NSE was too sensitive.

After the calibration, model validation was performed for a period different to the calibration period. Model performance in the validation was represented by *NSE* for water balance and *RMSE* for isotope balance, as well as in the calibration.

3.4 Estimation of time-variant MTT

To estimate time-variant MTT using a calibrated/validated tank model, a virtual (or imaginary) "age" tracer was introduced into the model (such an approach has been attempted previously by Goode (1996) for groundwater and Khatiwala et al. (2001) for oceans).

If we define the age as the time elapsed from the water entering the catchment across the ground surface, then $A(1) = 0$ throughout the simulation period. Solving $A(i)$ under this boundary condition means that the value of $A(i)$ indicates the mean age of the water in each tank and therefore, MTT (A_Q) can be predicted as:

$$A_Q = \frac{\sum_{i=1}^{5} q_H(i) A(i)}{Q}, \tag{17}$$

where, if we take a time step of one day, the units of $A(i)$ and A_Q are days, and the final term, which is unity, indicates the rate of ageing (Fig. 2). The concentration of this conservative and non-reactive tracer $A(i)$ is computed by

$$\Delta A(i) = \frac{q_V(i-1)A(i-1)dt - \left(q_V(i) + q_H(i) + f_T T_r + f_E E_S\right)A(i)dt}{h(i)} + 1 \qquad \text{for } i = 2\text{-}5. \tag{18}$$

4. Results and discussion

4.1 Water and isotope balance

The simulated discharge largely agrees with that observed (Fig. 3), although a few discrepancies exist. For example, some peaks of observed discharge could not be reproduced or were underestimated in the simulation, especially for SC1 and SC2 in 2006, SC3 in 2006 and 2009, SC4 in 2006–2007, and SC5 in 2006 and 2008. These discrepancies might be attributable to inaccuracies in the precipitation data used in the simulation, because the study catchments are mountainous with relatively large extent, such that the spatial distribution of precipitation is highly heterogeneous and difficult to observe accurately. Overestimations of discharge peaks (e.g., for all SCs in late 2009, SC1 in 2008, and SC3 in 2010) could also be attributed to the same cause. Conversely, underestimations (e.g., SC1, SC3, and SC4 in 2007) and overestimations (e.g., SC4 in 2008 and 2010) of simulated discharge in low flow periods seem to be introduced by errors not just in precipitation, but also evapotranspiration. In the simulation, hydro-meteorological data observed at a few stations were used, such that it is difficult to represent precisely the fields of temperature, wind speed, and solar radiation for the entire catchment.

According to Moriasi et al. (2007), simulation results can be considered satisfactory if *NSE* is more than 0.36. In our results, *NSE* ranges from 0.3 to 0.6 in most cases, although those for SC1 and SC4 in 2008 and for SC3 in 2009 are less than 0.1 (Table 1). And, the ratio of simulated runoff compare observed ones are around 88.7% for the five catchments. Low performance in these specific cases is probably associated with inaccuracies in the precipitation data and evapotranspiration estimations. It is undeniable that limitation exist for a lumped model to reproduce these entire events precisely, especially for meso-scale catchment with complicated characters on daily step. However, the model used in this study is

shown capable of reproducing the water balance in all five SCs reasonably well.

A water balance simulation or simulated discharge is closely related to the 'change' in water storage, but is less sensitive to the water storage itself. However, an isotope balance simulation is closely related and thus more sensitive to the absolute value of water storage. Therefore, better performance of an isotope balance simulation can be linked to better estimation of transit time. Generally, the model in this study reproduced well both $\delta^{18}O$ and δD of river water in the five SCs (Fig. 4). However, as in water balance simulation, both overestimations and underestimations can be found. One possible reason for the lower isotope ratios in winter for some catchments might be snow melting, which was not considered in this model. Also, rough estimations of evaporation and transpiration might be another reason. Relatively large differences between the observed and simulated values exist, especially in the winter of 2011–2012 (excluding SC4), which might be caused by the spatial heterogeneity of precipitation isotope data. For the simulations, precipitation isotope data were obtained only at the Kofu site and were corrected considering catchment mean elevation, although spatial heterogeneity caused by factors other than elevation was not considered. Thus, this could in part be the cause of the observation–simulation differences.

The *RMSE* ranges from 0.17–1.17‰ for $\delta^{18}O$ and from 1.1–8.8‰ for δD (Table 1b). Surprisingly, the *RMSE* is smaller in the validation than in the calibration, suggesting that the model used is valid, but that its performance depends on the inter-annual changes in hydro-meteorological and/or isotopic conditions. In the case of validation, the *RMSE* of $\delta^{18}O$ (δD) is not greater than 0.57‰ (3.6‰). As the measurement error of $\delta^{18}O$ (δD) is 0.1‰ (1‰), as mentioned before, the isotope balance simulation in this study can be regarded as acceptable. Unfortunately, because the temporal resolution of isotope monitoring in this study is one month, the reproducibility of isotope variability in river water over shorter timescales is not sufficiently validated. If isotope data with greater temporal resolution were used, the accuracy of the model

might be improved further. Snow coverage and melting processes were not considered in this model, because the areal fraction of snow coverage is very small and yearly varied. Although there is an undeniable isotopic effect caused by snow melting, especially for the winter and early spring river isotopic composition, the influence is expected to be limited in considering with amounts of river water and snowmelt water.

4.2 Temporal variation of MTT and its precipitation dependence

Fig. 5 represents the MTT variations for SC1–SC5 with total catchment average precipitation for about ten years. While the MTT was originally computed in daily time steps, monthly averages are shown in this figure. The monthly average MTT ranges from several years to decades; the variation range, as well as the long-term average of MTT (LAMTT), differ for each SC (Table 2). The standard deviation (SD) and coefficient of variation (CV) are lowest in SC4 and highest in SC2 and SC5. And, LAMTT is lowest in SC1 (8.0 y) and highest in SC3 (16.5 y). The temporal variation patterns of MTT are similar among all the SCs. As the precipitation amount increases, the MTT becomes smaller; high values of MTT can be found during relatively dry periods. The annual cycle of MTT variation is clear, reflecting the seasonal variation of precipitation amount.

An inverse relationship between MTT and precipitation amount is clearly shown in Fig. 6. The determination coefficients (R^2) of the regression curves range from 0.43 (SC1) to 0.87 (SC4). The MTT values are almost the same for all SCs when the amount of monthly precipitation is large, while inter-catchment variation of MTT is exaggerated in dry periods. In other words, large storm events (i.e., high flow conditions), which introduce new water with the same age, tend to erase or weaken inter-catchment variation of MTT. Exponential regression was chosen for the better fitness than other regressions. However,

the equation does not provide enough matches for the large precipitations, which event account for less percentage. One possible reason for this behavior might because that, processes and forming mechanism of extreme precipitations, and the responses of catchments are different with normal precipitations.

4.3 Spatial variation of MTT and its controlling factors

As mentioned in the previous section, the temporal variation of MTT is caused mainly by precipitation, and the dependence of MTT on precipitation differs for each SC. Thus, it is worth investigating which factor(s) controls the spatial (i.e., inter-catchment) variability of MTT. Table 3 summarizes the correlations between LAMTT and the potential controlling factors: area (i.e., catchment size), topography, geology, land use/cover, and soil. As water storage within the catchment is expected to control MTT (especially for its inter-catchment variation), the water storage volume in each layer of the tank is also added as a potential factor. The correlation coefficient (R) is relatively high for the storage of Layer 4 (0.93), coverage of range grass (0.91), coverage of forest (−0.89), coverage of agriculture (0.79), coverage of Ss (sand–shale conglomerate of Mesozoic age; 0.80), and tangent of mean slope (−0.67). Fig. 7 displays scatter plots of LAMTT versus selected factors. In this figure, range grass and agriculture were excluded, because their percentages were relatively small and inversely correlated closely with forest coverage, which accounts for 67% to 94% in each SC.

Hrachowitz et al. (2010) have shown that variance of MTT decreases with increasing catchment size and that MTTs in larger downstream catchments tend to converge. In the present study, a close relationship between LAMTT and catchment size could be found for SCs1–4 (Fig. 7a). However, SC5 did not obey this relationship and displayed an intermediate LAMTT compared with those of the upstream SCs. As a result, its correlation coefficient of MTT versus catchment area is relatively small.

Soulsby et al. (2006b) showed a positive correlation between MTT and mean slope within the catchment, while McGuire et al. (2005) found a negative correlation of MTT versus median flowpath gradient. In the present study, MTT is inversely correlated with mean slope (Fig. 7b); however, the correlation coefficient is smaller than that for some other factors.

Many previous studies (Soulsby et al., 2006a, b; Tetzlaff et al., 2009; Hrachowitz et al., 2010) have highlighted that MTT decreases with increasing areal percentage of responsive soil cover (i.e., regosols, peats, and gleys) within a catchment. However, in the present study, the correlation of MTT is not significant with the coverage of any specific soil. Conversely, the areal percentage of forest and Ss show strong correlation with MTT (Fig. 7c and d), whereas previous studies have never emphasized relationships between MTT and specific land use/cover or geology.

The highest correlation was found between MTT and the storage amount of Layer 4 (Fig. 7e). Although the lumped hydrologic model used in this study is a semi-conceptual one, Layer 4 implicitly corresponds to groundwater storage. Soulsby et al. (2006b) clarified that MTT increases with increasing groundwater contribution to a stream and our results are consistent with their finding.

As mentioned above, the factors likely to control MTT are storage of Layer 4, forest coverage, Ss coverage, and mean slope; however, some factors correlate with each other (Table 4). To clarify the independent (i.e., true) controlling factor(s), multiple linear regression (MLR) with a stepwise selection of explanatory variables was applied. The first and second best MLR models were as follows:

$$MTT = 0.358S_{L4} + 0.189C_{Ss} + 4.613 \qquad \text{(Adjusted-}R^2 = 0.988\text{)} \qquad (19)$$

$$MTT = 0.471S_{L4} + 4.866 \qquad \text{(Adjusted-}R^2 = 0.828\text{)} \qquad (20)$$

where S_{L4} (m) is the storage of Layer 4 and C_{Ss} (m^2/m^2) is the Ss coverage. This result suggests that the most important factor controlling LAMTT is the storage of Layer 4, i.e., groundwater storage. In mountainous areas, where mean slope is high and the dominant land use/cover is forest, good aquifers are thin and thus, groundwater storage is expected to be small. Conversely, in the plains, groundwater storage seems to be greater because of the thicker aquifers compared with mountainous areas. Large groundwater storage helps water to age, which increases transit times.

The Ss coverage, which is the second important variable in the MLR models, is much higher in SC2 than in the other SCs. In SC2, some tributaries of the Fuji River have formed alluvial fans with very thick sediments, which are mainly composed of highly permeable sand–shale conglomerate. In such a catchment, deep flowpaths through the thick sediments are expected to contribute considerably to river runoff. Indeed, as for the model, the value of k_V of Layer 4 in SC2 is the largest among all the SCs, strengthening deep flowpaths. This indicates that groundwater contributions to river runoff in SC2 are represented not only by Layer 4, but also by Layer 5. In other words, groundwater flow patterns in alluvial-fan-dominated catchments seem to differ from those in other catchments. This is the reason why Ss coverage is the second important factor, independent of the storage of Layer 4.

In short, groundwater storage is undoubtedly important as a factor controlling inter-catchment variation of LAMTT. As shown in the previous section, inter-catchment variation of LAMTT reflects the difference of MTT in dry periods more strongly. Although inter-catchment variation in wet periods could be affected by other factors, such effects should be minor because the spatial variance of MTT in wet periods is small.

In previous studies, the importance of both groundwater storage and its topographic control has not been

emphasized. This is probably because small headwater catchments dominated by mountainous topography have been the principal focus of study and few mesoscale catchments that include plains with large groundwater storage have been investigated. In this context, the most dominant factor controlling the spatial variation of MTT might be scale-dependent, even though catchment size is not a direct controlling factor.

5. Summary and conclusions

Time-variant MTTs of five SCs of the Fuji River catchment were estimated using a five-layer tank model, calibrated and validated using observed river discharge and river water stable isotopes (i.e., $\delta^{18}O$ and δD). The monthly average MTTs ranged from several years to decades; the variation range and long-term averages were different for all the SCs. However, the patterns of temporal variation of the estimated MTTs were similar in all SCs. Inter-catchment variation of MTT was greater in dry periods than in wet periods. The long-term average MTT in each SC was correlated with mean slope, coverage of forest (or conversely, other land use types), coverage of sand–shale conglomerate, and groundwater storage. The use of multiple linear regression revealed that inter-catchment variation of MTT is principally controlled by the amount of groundwater storage, which is smaller in mountainous areas covered mostly by forests than in plain areas with less forest coverage and smaller slopes. Such topographic control of MTT through the factor of groundwater storage seems important in mesoscale catchments that include both mountains and plains.

To a greater or lesser extent, model-based estimates of MTT depend on the structure and/or accuracy of the model. River discharge and river water isotopic compositions were well reproduced by the model, not only in calibration periods, but also in the validation periods. Furthermore, the fact that inter-catchment

variation of MTT could be reasonably explained by catchment characteristics (e.g., topography, land use, and geology) and internal parameters of the model (e.g., storage of Layer 4) supports the usefulness of our approach. As the MTT is more strongly controlled by water storage than by flow, isotopic tracers sensitive to water storage are shown to be important tools for calibrating/validating the model.

Acknowledgments

This study was supported in part by the Research and Education Funding for Japanese Alps Inter-Universities Cooperative Project, Ministry of Education, Culture, Sports, Science and Technology, Japan, and Japan Society for the Promotion of Science (JSPS) KAKENHI Grant Number 25·3813. The authors would like to acknowledge Professor Jeff McDonnell for his invaluable suggestions. Comments from the two anonymous reviewers were helpful in improving our manuscript.

References

Allen, R.G., Pereira, L.S., Raes, D. and Smith, M., 1998. Crop evapotranspiration: guidelines for computing crop requirements, FAO Irrigation and Drainage Paper No. 56, FAO, Rome, Italy.

Blöschl, G., 2005. On the Fundamentals of Hydrological sciences, Encyclopedia of Hydrological Sciences. 3471, 3–12.

Bolin, B., Rodhe, H., 1973. A note on the concepts of age distribution and transit time in natural reservoirs, Tellus. 25, 58–62.

Cappa, C.D., Hendricks, H.B., Depaolo, D.J., Cohen, R.C., 2003. Isotopic fractionation of water during evaporation. J. Geophys. Res. 108, D16–4525, doi:10.1029/2003JD003597.

Craig, H., Gordon, L.I., 1965. Deuterium and oxygen 18 variations in the ocean and marine atmosphere. In proc. Stable Isotopes in Oceanographic Studies and Paleotemperatures, Tongiogi, E. (Eds.), pp. 9–130, V. Lishi e F., Pisa, Spoleto, Italy..

DeWalle, D.R., Edwards, P.J., Swistock, B.R., Aravena, R., Drimmie, R.J., 1997. Seasonal isotope hydrology of three Appalachian forest catchments, Hydrol. Process. 11(15), 1895–1906.

Druhan, JL., Maher, K., 2014. A model linking stable isotope fractionation to water flux and transit times in heterogeneous porous media. Procedia Earth and Planetary Science 10, 179–188, doi:10.1016/j.proeps.2014.08.054.

Duffy, C.J., 2010. Dynamical modeling of concentration–age–discharge in watersheds, Hydrol. Process. 24, 1711–1718.

Fovet, O., L. Ruiz, L., Faucheux, M., Molénat, J., Sekhar, M., Vertès, F., Aquilina, L., Gascuel-Odoux, C., and Durand, P., 2014. Using long time series of agricultural-derived nitrates for estimating catchment transit times, J. Hydrol. 522(2015), 603–617, doi:10.1016/j.jhydrol.2015.01.030.

Gat, J.R., Shemesh, A., Tziperman, E., Hecht, A., Georgopoulos, D., Basturk, O., 1996. The stable isotope composition of waters of the eastern Mediterranean Sea. J. Geophys. Res. 101(C3), 6441–6452, doi:10.1029/95JC02829.

Goode, D.J., 1996. Direct simulation of groundwater age. Water Resour. Res. 32(2), 289–296.

Hrachowitz, M., Soulsby, C., Tetzlaff, D., Speed, M., 2010. Catchment transit times and landscape controls–does scale matter? Hydrol. Process. 24(1), 117–125.

Hrachowitz, M., Fovet, O., Ruiz, L., and Savenije, H. H. G., 2015. Transit time distributions, legacy

contamination and variability in biogeochemical 1/fα scaling: how are hydrological response dynamics linked to water quality at the catchment scale?. Hydrol. Process., doi: 10.1002/hyp.10546.

Khatiwala, S., Visbeck, M., Schlosser, P., 2001. Age tracers in an ocean GCM, Deep-Sea Res.Pt. 48, 1423–1441.

Kim, S. and Jung, S., 2014, Estimation of mean water transit time on a steep hillslope in South Korea using soil moisture measurements and deuterium excess. Hydrol. Process., 28,1844–1857, doi: 10.1002/hyp.9722.

Klaus, J., Chun, K., McGuire, K., McDonnell, J.J., 2015. Temporal dynamics of catchment transit times from stable isotope data. Water Resources Research, 51, 4208–4223, doi:10.1002/ 2014WR016247.

Kubota, T., Tsuboyama, Y., 2004. Estimation of evaporation rate from the forest floor using oxygen-18 and deuterium compositions of throughfall and stream water during a non-storm runoff period, Journal of Forest Research. 9, 51–59.

Love, D., Uhlenbrook, S., Zaag, P., 2011. Regionalising a meso-catchment scale conceptual model for river basin management in the semi-arid environment, Physics and Chemistry of the Earth. 36, 747–760. doi:10.1016/j.pce.2011.07.005.

Ma, W., Yamanaka, T., 2013. Temporal variability of mean transit time and transit time distribution assessed by a tracer-aided tank model for a meso-scale catchment, Hydrological Research Letters. 7(4), 104–109, doi: 10.3178/hrl.7.104.

Makino, Y. (2013), Mapping of Stable Isotopes in Precipitation over the Japanese Alps Region and Its Use for Diagnosing Hydrological Cycle for Catchment Area, M.S. thesis, 81 pp., Univ. of Tskuba. at Tsukuba, Japan, 28 February.

Majoube, M., 1971. Fraction0nement en oxygene-18 entre la glace et la vapeur d'eau. J. Chim. Phys. 68,

625–636.

Makihara, Y., 1996. A method for improving radar estimates of precipitation by comparing data from radars and raingauges. J. Meteor. Soc. Japan. 74, 459–480.

Maloszewski, P., Zuber, A., 1982. Determining the turnover time of groundwater systems with the aid of environmental tracers, I-Models and their applicability. J. Hydrol. 57, 3–4. 207–231.

Maloszewski, P., Rauert, W., Stichler, W., Herrmann, A., 1983. Application of flow models in an alpine catchment area using tritium and deuterium data. J. Hydrol. 66, 319–330.

McDonnell, J.J., McGuire, K., Aggarwal, P., Beven, K.J., Biondi, D., Destouni, G., Dunn, S., James, A., Kirchner, J., Kraft, P., Lyon, S., Maloszewski, P., Newman, B., Pfister, L., Rinaldo, A., Rodhe, A., Sayama, T., Seibert, J., Solomon, K., Soulsby, C., Stewart, M., Tetzlaff, D., Tobin, C., Troch, P., Weiler, M., Western, A., W¨orman, A., Wrede, S., 2010. How old is stream water? Open questions in catchment transit time conceptualization, modeling and analysis. Hydrol. Process. 24, 1745–1754.

McGuire, K.J., DeWalle, D.R., Gburek, W.J., 2002. Evaluation of mean residence time in subsurface waters using oxygen-18 fluctuations during drought conditions in the mid-Appalachians. J. Hydrol. 261(1–4), 132–149.

McGuire, K.J., McDonnell, J.J., Weiler, M., Kendall, C., Welker, J.M., McGlynn, B.L., Seibert, J., 2005. The role of topography on catchment-scale water residence time. Water Resour. Res. 41(5), W05002, doi:10.1029/2004WR00365.

McGuire, K.J., McDonnell, J.J., 2006. A review and evaluation of catchment transit time modeling. J. Hydrol. 330(3-4), 543–563.

Moriasi, D.N., Arnold, J.G., Van Liew, M.W., Bingner, R.L., Harmel, R.D., Veith, T.L., 2007. Model Evaluation Guidelines for Systematic Quantification of Accuracy in Watershed Simulations,

Transactions of the ASABE. 50(3), 885–900.

Muñoz-Villers, L., Geissert, D., Holwerda, F., and McDonnell, J. J., 2015. Stream water transit times in tropical montane watersheds: catchment scale and landscape influences. Hydrol. Earth Syst. Sci. Discuss., 12, 10975–11011, doi:10.5194/hessd-12-10975-2015.

Nash, J.E., Sutcliffe, J.V., 1970. River flow forecasting through conceptual models part I-A discussion of principles, J. Hydrol. 10(3), 282–290.

Ozyurt, N.N., Bayari, C.S., 2003. LUMPED: a Visual Basic code of lumped-parameter models for mean residence time analyses of groundwater systems, Computers & Geosciences. 29, 79–90, doi:10.1016/S0098-3004(02)00075-4.

Peters, NE., Burns, DA., Aulenbach, BT., 2014. Evaluation of High-Frequency Mean Streamwater Transit-Time Estimates Using Groundwater Age and Dissolved Silica Concentrations in a Small Forested Watershed. Aquat Geochem. 20, 183–202, doi:10.1007/s10498-013-9207-6.

Sayama, T., McDonnell, J.J., 2009. A new time-space accounting scheme to predict stream water residence time and hydrograph source components at the watershed scale, Water Resour. Res. 45, W07401, doi:10.1029/2008WR007549.

Scherrer, S., Naef, F., 2003. A decision scheme to indicate dominant hydrological flow processes on temperate grassland. Hydrol. Process. 17(2), 39–401.

Seeger, S., Weiler, M., 2004. Reevaluation of transit time distributions, mean transit times and their relation to catchment topography, Hydrol. Earth Syst. Sci., 18, 4751-4771, doi:10.5194/hess-18-4751-2014, 2014.

Shimada, J., Itadera, K., Nakai, N., Suprapta, DN., Gara, W., 1992. Stable isotope ratio in precipitation as an input of hydrological cycle. In Water Cycle and Water Use in Bali Island, Kayane I (ed.). University of

Tsukuba: Tsukuba; 105–115.

Soulsby, C., Tetzlaff, D., Dunn, S.M., Waldron, S., 2006a. Scaling up and out in runoff process understanding-Insights from nested experimental catchment studies, Hydrol. Process. 20, 2461–2465, doi:10.1002/hyp.6338. 2006.

Soulsby, C., Tetzlaff, D., Rodgers, P., Dunn, S., Waldron, S., 2006b. Runoff processes, stream water residence times and controlling landscape characteristics in a mesoscale catchment: an initial evaluation. J. Hydrol. 325, 197-221.

Stockinger, M. P., Bogena, H. R., Lücke, A., Diekkrüger, B., Weiler, M., and Vereecken, H., 2014. Seasonal soil moisture patterns: Controlling transit time distributions in a forested headwater catchment, Water Resour. Res. 50, 5270–5289, doi:10.1002/ 2013WR014815.

Sugita, M., Tanaka, T., 2009. Hydrologic Science, Kyoritsu Shuppan Co, Japan, pp. 275.

Tetzlaff, D., Seibert, J., Soulsby, C., 2009. Inter-catchment comparison to assess the influence of topography and soils on catchment transit times in a geomorphic province. Hydrol. Process. 23(13), 1847–1886.

Tetzlaff, D., Birkel, C., Dick, J., Geris, J., and Soulsby. C., 2014. Storage dynamics in hydropedological units control hillslope connectivity, runoff generation, and the evolution of catchment transit time distributions, Water Resour. Res., 50, 969–985, doi: 10.1002/2013WR014147.

Timbe, E., Windhorst, D., Celleri, R., Timbe, L., Crespo, P., Frede, H. G., Feyen, J., and Breuer, L., 2015. Sampling frequency trade-offs in the assessment of mean transit times of tropical montane catchment waters under semi-steady-state conditions, Hydrol. Earth Syst. Sci., 19, 1153–1168, doi:10.5194/hess-19-1153-2015.

Uhlenbrook, S., Roser, S., Tilch, N., 2004. Hydrological process representation at the meso-scale: the potential of a distributed, conceptual catchment model. J. Hydrol. 291, 278–296

Yamanaka, T., Shimada, J., Hamada, Y., Tanaka, T., Yang, Y., Wanjun, Z., and Chunsheng, H., 2004. Hydrogen and oxygen isotopes in precipitation in a northern part of the North China Plain: Climatology and inter-storm variability. Hydrol. Process. 18, 2211- 2222.

Yamanaka, T., 2009. Study on the atomspheric boundary layer using water vapor isotopes. K. Yoshimura, K. Ichiyanagi and A. Sugimoto (Eds): "Use of Isotope Ratios of Water in Meteorology", Meteorological Society of Japan, 61–76, Tokyo, Japan.

Yamanaka T., Onda Y., 2011. On measurement accuracy of liquid water isotope analyzer based on wavelength-scanned cavity ring-down spectroscopy (WSCRDS). Bulletin of Terrestrial Environment Research Center, University of Tsukuba, 12, 31–40.

Figures:

Fig. 1. Map of study area and locations of isotopic monitoring sites and meteorological observation stations. Here, Y1-Y5 represent isotopic collecting location. And, W1-W5 shows location of the Weather Station, from where, meteorological observed data were collected, such as: temperature, precipitation, wind, solar and others. 29

Fig. 2. Schematic illustration of five-layer tank model. 30

Fig. 3. Comparison between observed and simulated hydrographs..... 31

Fig. 4. Comparison between observed and simulated isotope compositions..... 32

Fig. 5. Comparison of MTT in monthly values among five SCs as well as monthly average precipitation for the whole research area (i.e. SC5). 33

Fig. 6. Inter-catchment comparison of relationships between monthly average MTT and precipitation amount for five SCs. 34

Fig. 7. Relationships of LAMTT with potential controlling factors in each SC. 35

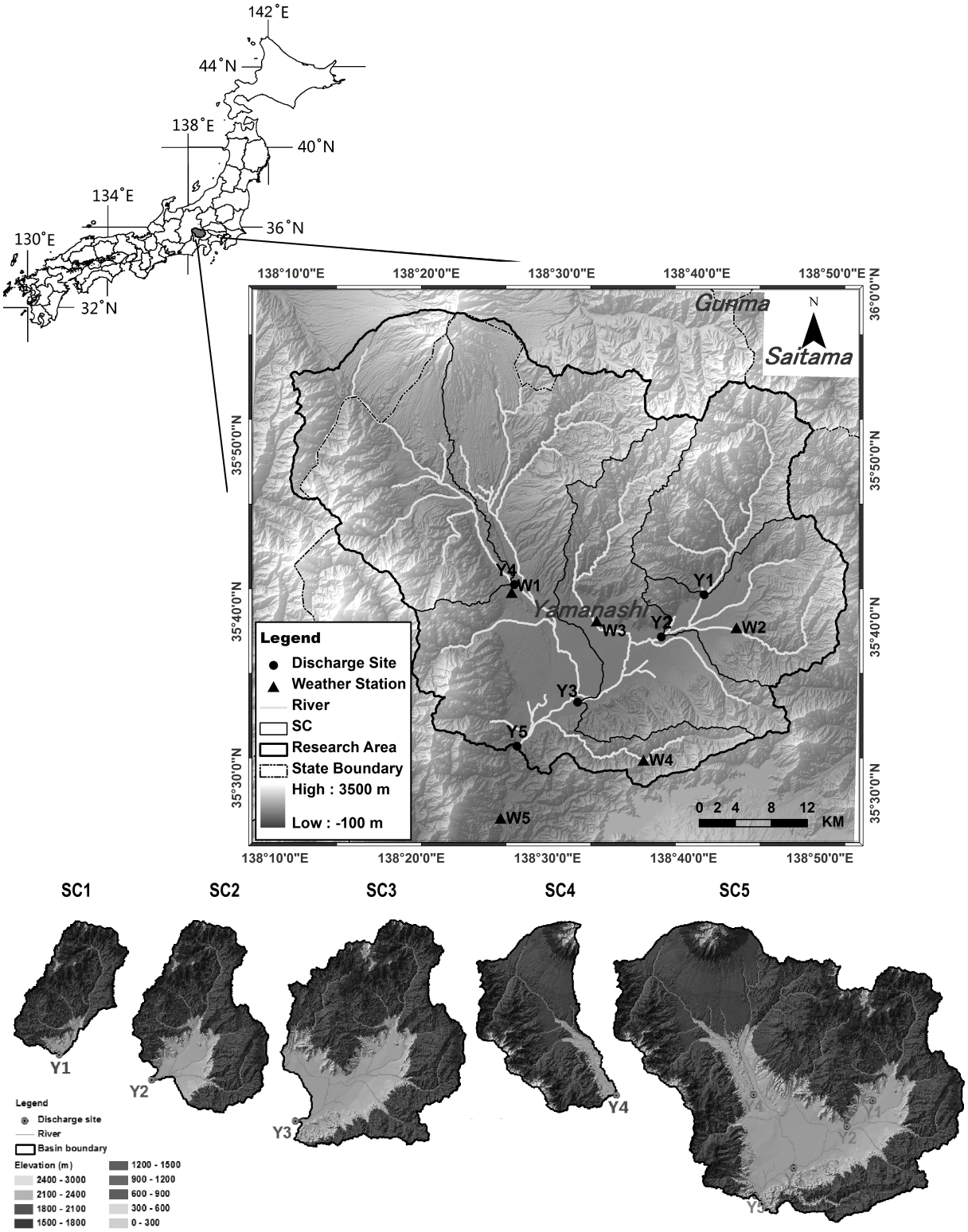

Fig. 1. Map of study area and locations of isotopic monitoring sites and meteorological observation stations. Here, Y1-Y5 represent isotopic collecting location. And, W1-W5 shows location of the Weather Station, from where, meteorological observed data were collected, such as: temperature, precipitation, wind, solar and others.

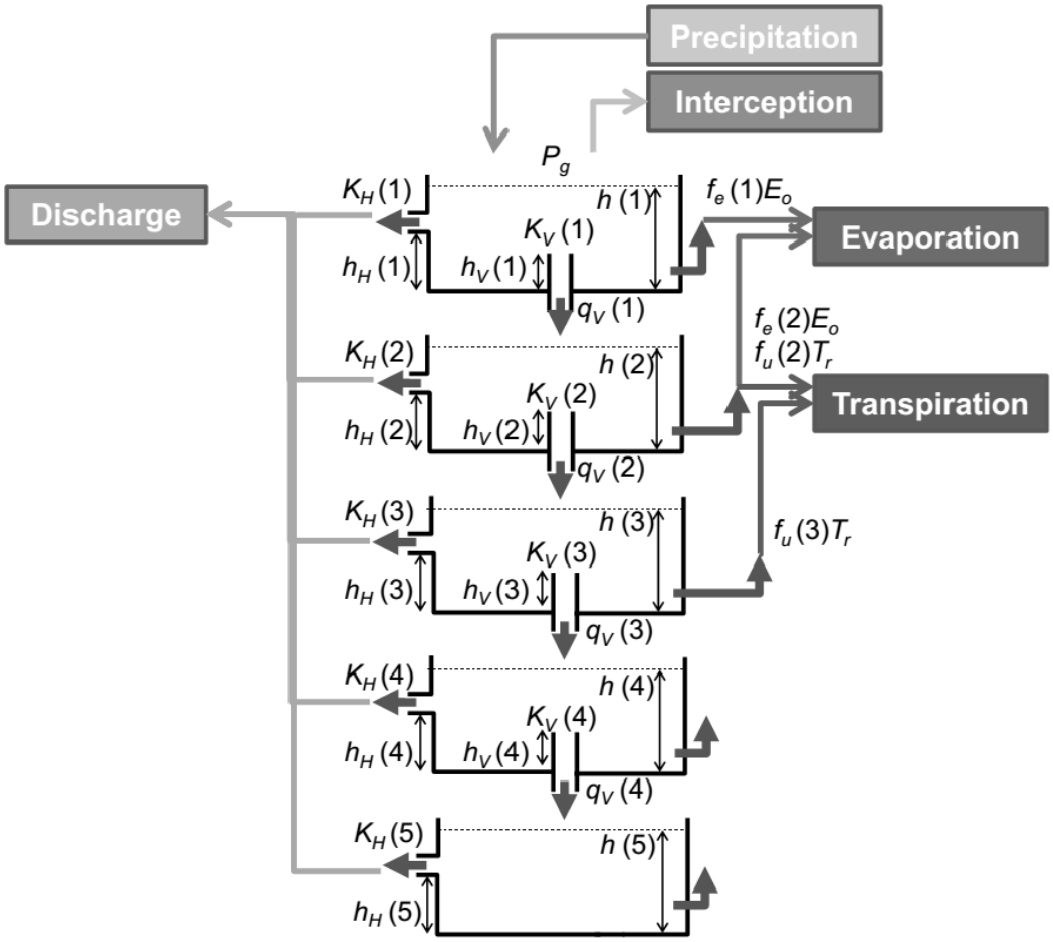

Fig. 2. Schematic illustration of five-layer tank model.

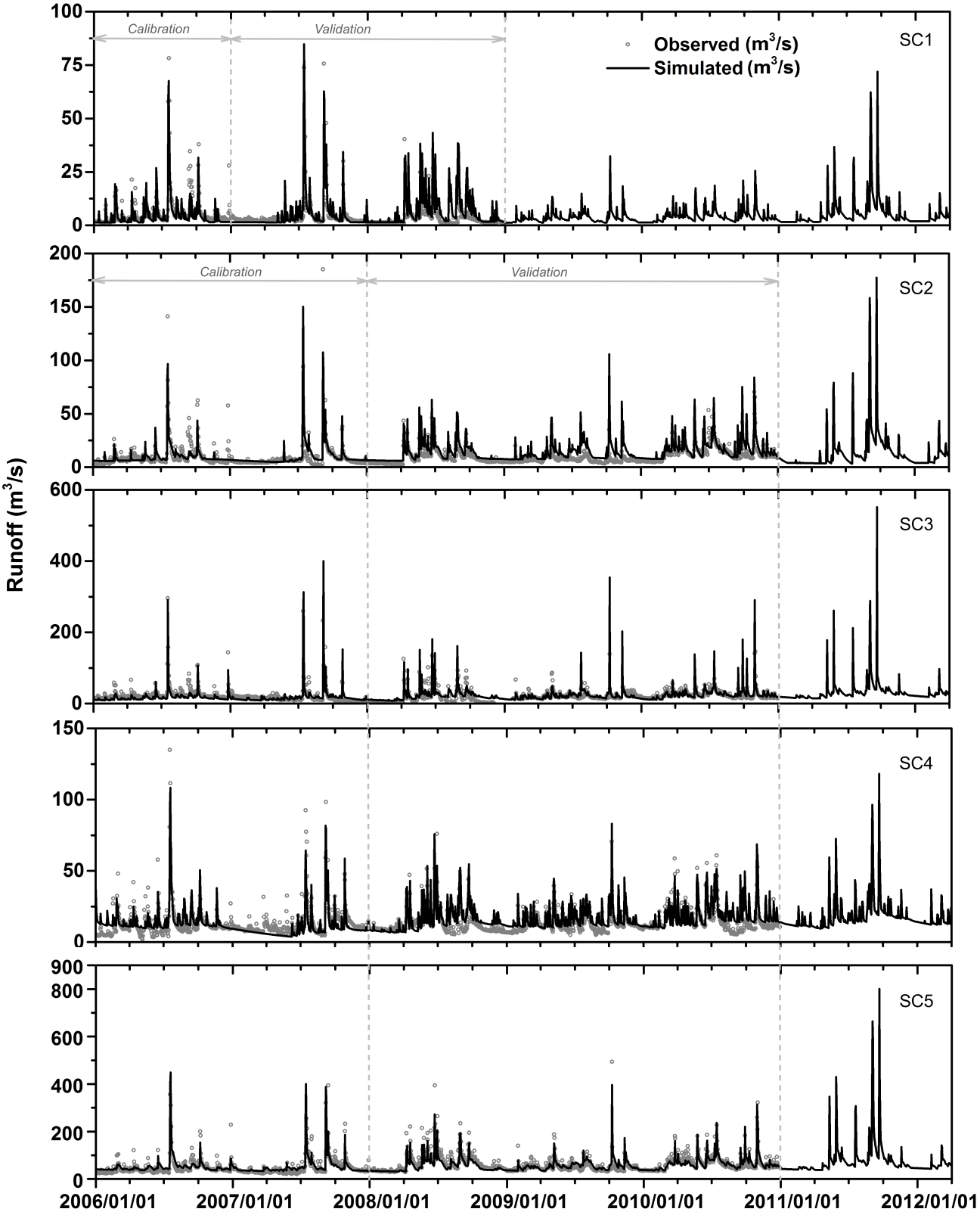

Fig. 3. Comparison between observed and simulated hydrographs.

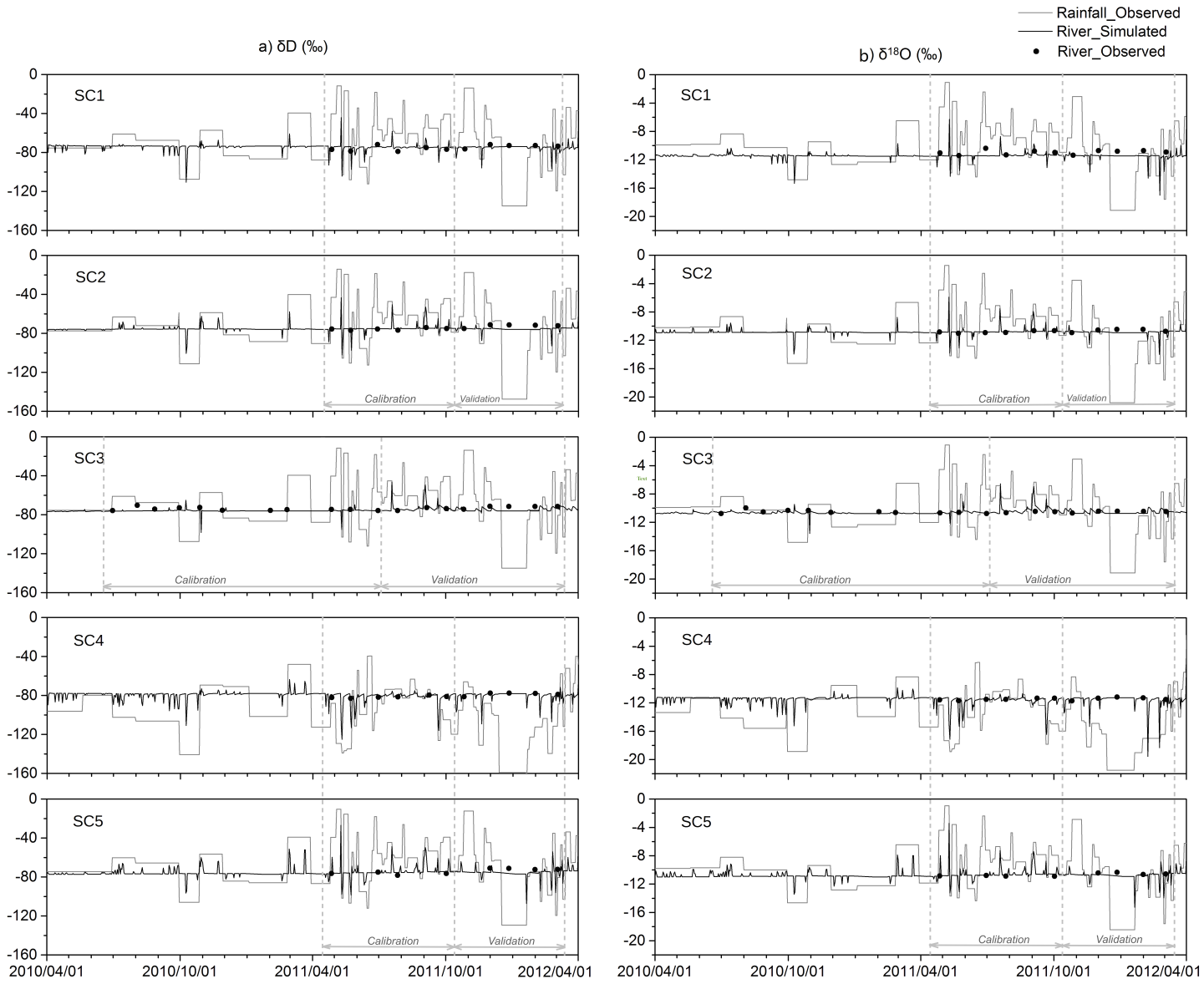

Fig. 4. Comparison between observed and simulated isotope compositions.

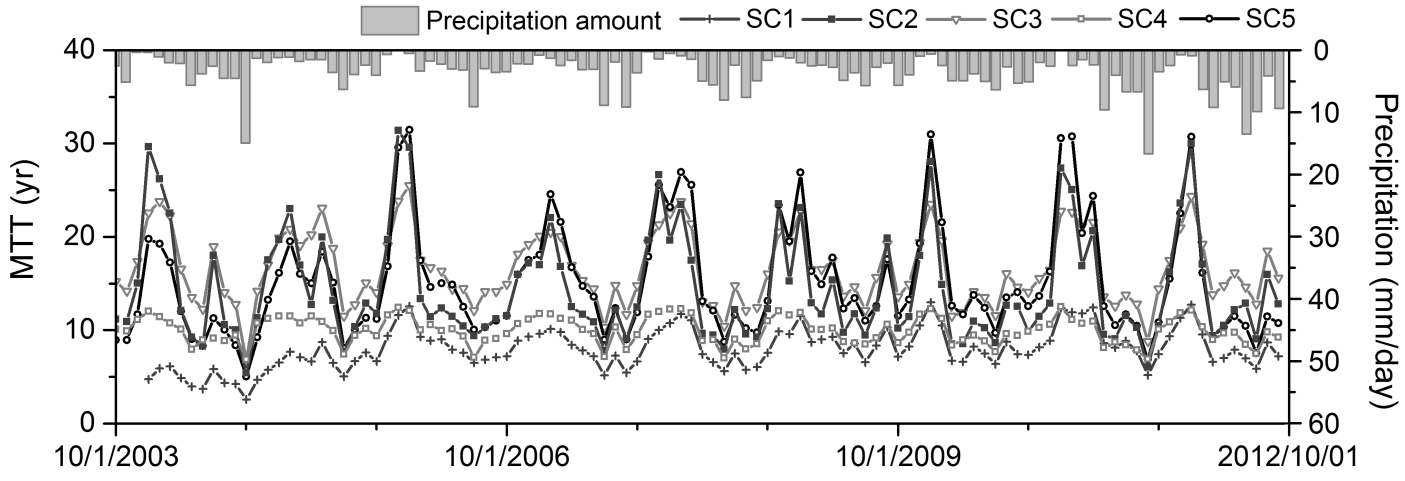

Fig. 5. Comparison of MTT in monthly values among five SCs as well as monthly average precipitation for the whole research area (i.e. SC5).

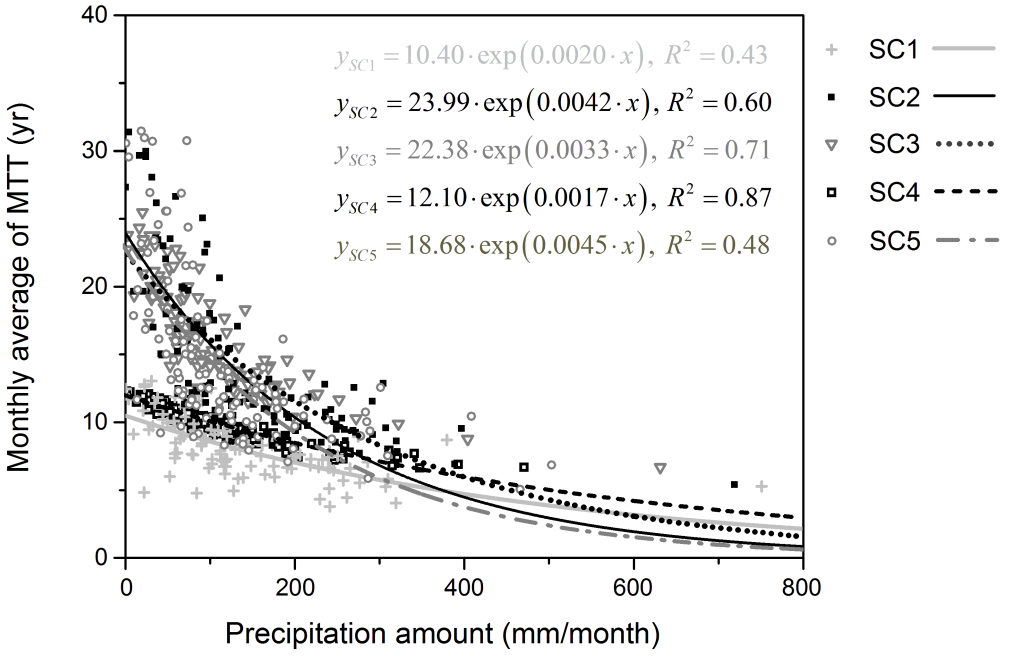

Fig. 6. Inter-catchment comparison of relationships between monthly average MTT and precipitation amount for five SCs.

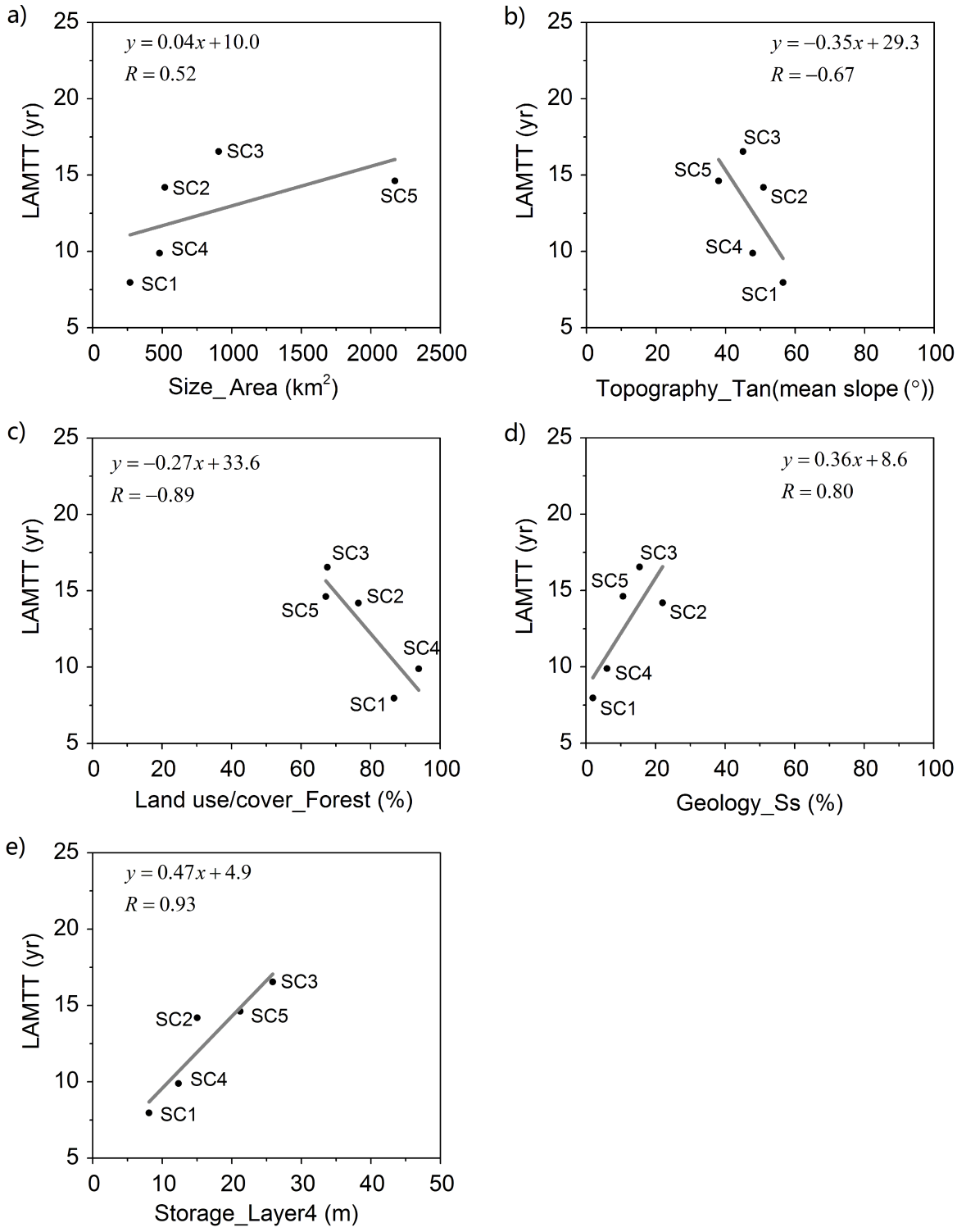

Fig. 7. Relationships of LAMTT with potential controlling factors in each SC.

ɘ
)

Tables:

Table 1. Characters of each catchment. 38

Table 2. Evaluation for simulations of (a) water balance and (b) isotope balance. 39

Table 3. Long-term statistics of estimated mean transit time on daily bases. 40

Table 4. Coefficients of correlation of LAMTT and potential controlling facotrs in each SC. 41

Table 5. Correlation matrix among potential factors controlling MTT 42

3 Table 1. Characters of each catchment.

		SC1	SC2	SC3	SC4	SC5
Elevation (m)		1211.1	615.6	448	2455.4	376.2
Area (km^2)		268	518.5	905.7	480.3	2172.7
Slope (%)	0~3˚	2.03	9.49	16.21	6.8	1.06
	3~5˚	1.58	2.65	3.35	10.28	14.65
	5~8˚	2.93	3.83	3.99	10.25	6.39
	8~15˚	9.38	9.48	9.86	10.93	17.62
	15~25˚	21.32	19.02	18.62	13.73	16.46
	25~30˚	14.94	12.86	11.7	8.88	10.04
	30~45˚	41.67	37.06	31.69	30.57	28.49
	45~60˚	6.08	5.56	4.53	8.22	5.16
	60~75˚	0.07	0.05	0.05	0.33	0.12
	75˚~	0	0	0	0.01	0
	Weighted	28.6	25.78	23.01	23.63	22.57
Land use (%)	Forest	86.71	76.46	67.55	93.84	67.11
	Agriculture	8.29	15.53	16.14	0.44	13.31
	Residence	1.78	1.24	1.78	1.03	2.87
	Range grass	1.93	4.47	7.44	2.84	6.02
	Transportation	0.03	0.22	0.48	1.74	0.46
	Water	0.50	1.22	1.99	0.11	2.21
	Institution	0.06	0.16	0.74	-	0.93
	Rice	0.49	0.59	3.21	-	6.52
	Pasture	-	0.12	0.66	-	0.57
Geology (%)	Ba	77.67	61.17	45.13	2.99	22.17
	Wf	17.85	13.91	19.72	7.11	16.04
	Ss	1.95	22.01	15.37	6.04	10.64
	Gr	2.54	1.31	2.33	20.43	5.54
Soil types (%)	Brown forest soil	57.06	73.00	67.98	75.20	49.55
	Podsol	5.51	6.49	5.65	12.39	10.47
	Andosol	17.70	7.89	8.66	3.57	28.48
	Lithosol	2.41	1.47	1.12	2.78	5.40
	Rocky land	1.11	0.57	0.46	1.09	1.50
	Red yellow soil	4.38	5.21	5.58	4.37	
	Gley soil	2.08		1.99		
	Others	0.69		0.09		1.03

Table 2. Evaluation for simulations of (a) water balance and (b) isotope balance.

(a)

	SC1		SC2		SC3		SC4		SC5	
	Period	NSE	Period	NSE	Period	NSE	Period	NSE	Period	NSE
Calibration	*2006*	0.27	*2006-2007*	0.43	*2006-2007*	0.37	*2006-2007*	0.50	*2006-2007*	0.603
Validation	*2007*	0.34	*2008*	0.33	*2008*	0.40	*2008*	0.06	*2008*	0.57
	2008	0.01	*2009*	0.06	*2009*	0.22	*2009*	0.40	*2009*	0.34
			2010	0.29	*2010*	0.30	*2010*	0.31	*2010*	0.49

(b)

		Period	RMSE ($\delta^{18}O$)	RMSE (δD)	RMSE ($(\delta D/8+ \delta^{18}O)/2$)
SC1	Calibration	2011.04-2011.10	0.54	4.6	0.56
	Validation	2011.11-2012.03	0.57	1.8	0.40
SC2	Calibration	2011.04-2011.10	1.00	7.1	0.95
	Validation	2011.10-2012.03	0.30	3.2	0.35
SC3	Calibration	2010.05-2011.07	0.23	1.6	0.24
	Validation	2011.08-2012.03	0.24	2.4	0.22
SC4	Calibration	2011.05-2011.10	1.17	8.8	1.08
	Validation	2011.11-2012.03	0.17	1.1	0.16
SC5	Calibration	2011.04-2011.10	0.21	1.9	0.23
	Validation	2011.11-2012.03	0.27	3.6	0.36

Table 3. Long-term statistics of estimated mean transit time on daily bases.

	SC1	SC2	SC3	SC4	SC5
Average (LAMTT, yr)	8.0	14.2	16.5	9.9	14.6
SD* (yr)	2.2	5.8	3.9	1.4	6.0
CV** (%)	27.3	40.7	23.6	14.6	41.1

*SD: Standard deviation;

**CV: Coefficient of variation

Table 4. Coefficients of correlation of LAMTT and potential controlling facotrs in each SC.

Indices		*R*
Size		
	Area	0.56
Topography		
	Elevation	0.07
	Tan(mean slope (˚))	-0.67
	Maxlength_river	0.56
Soil		
	Rocky land	-0.45
	Lithosol	-0.10
	Andosol	0.26
	Podsol	-0.45
	Brown forest soil	0.02
Land use/cover		
	Range grass	0.91
	Transportation	-0.19
	Residence	0.33
	Agriculture	0.79
	Forest	-0.89
Geology		
	Wt	0.39
	Ss	0.80
	Ba	-0.13
	Gr	-0.40
Storage		
	Layer 1	0.40
	Layer 2	-0.10
	Layer 3	0.35
	Layer 4	0.93
	Layer 5	0.52

Table 5. Correlation matrix among potential factors controlling MTT.

	Storage_ Layer4	Land use/cover_ Forest	Geology_ Ss	Topography_ Tan(weighted slope)
Storage_Layer4	1.00	–	–	–
Land use/cover_Forest	-0.86	1.00	–	–
Geology_Ss	0.57	-0.58	1.00	–
Topography_ Tan(mean slope)	-0.77	0.64	-0.25	1.00